Atmos. Chem. Phys., 25, 2551–2568, 2025
https://doi.org/10.5194/acp-25-2551-2025

Atmospheric Chemistry and Physics
Open Access
EGU

Characterization of nitrous acid and its potential effects on secondary pollution in the warm season in Beijing urban areas

Junling Li[1], Chaofan Lian[2,a], Mingyuan Liu[3], Hao Zhang[1], Yongxin Yan[1], Yufei Song[1], Chun Chen[1], Jiaqi Wang[1], Haijie Zhang[1], Yanqin Ren[1], Yucong Guo[2], Weigang Wang[2], Yisheng Xu[1], Hong Li[1], Jian Gao[1], and Maofa Ge[2]

[1]State Key Laboratory of Environmental Criteria and Risk Assessment, Chinese Research Academy of Environmental Sciences, Beijing 100012, China
[2]State Key Laboratory for Structural Chemistry of Unstable and Stable Species, Beijing National Laboratory for Molecular Sciences (BNLMS), CAS Research/Education Center for Excellence in Molecular Sciences, Institute of Chemistry, Chinese Academy of Sciences, Beijing 100190, China
[3]China National Environmental Monitoring Centre, Beijing 100012, China
[a]now at: Assessment and Research Center for Pollution and Carbon Reduction, Tianfu Yongxing Laboratory, Chengdu 610213, China

Correspondence: Hong Li (lihong@craes.org.cn), Jian Gao (gaojian@craes.org.cn), and Maofa Ge (gemaofa@iccas.ac.cn)

Received: 7 February 2024 – Discussion started: 25 March 2024
Revised: 2 January 2025 – Accepted: 3 January 2025 – Published: 27 February 2025

Abstract. As a key source of hydroxyl (OH) radicals, nitrous acid (HONO) has attracted much attention for its important role in the atmospheric oxidant capacity (AOC) increase. In this study, we made a comparison of the ambient levels, variation patterns, sources, and formation pathway in the warm season (from June to October in 2021) on the basis of a continuous intensive observation in an urban site of Beijing. The monthly average mixing ratios of HONO were 1.3, 1.3, 1.0, 0.96, and 0.89 ppb, respectively, showing a larger contribution to OH radicals relative to ozone in the daytime. The emission factor (EF) relative to NO_x from the vehicle emissions was estimated to be 0.017, higher than most studies conducted in Beijing. The average nocturnal NO_2/HONO conversion frequency k_{HONO} was 0.008 h^{-1}. In the warm season, the missing source of HONO, $P_{unknown}$, around noontime was 0.29–2.7 ppb h^{-1}. According to the OH production from HONO, the OH production rate from the missing HONO was also very important to the AOC. This work highlights the importance of HONO for the AOC in the warm season, while encouraging long-term HONO observation to assess the contribution of HONO sources over time compared to the capture of pollution processes.

1 Introduction

From 2013 to 2022, the annual average concentration of $PM_{2.5}$ in China decreased, but it is still much higher than the World Health Organization's guideline value (5 µg m^{-3}). Ozone pollution, on the other hand, is becoming more and more prominent (Y. Liu et al., 2023; Li et al., 2022). China's air quality problem has developed from being dominated by $PM_{2.5}$ in the past to being affected by the photochemical pollutants $PM_{2.5}$ and ozone, that is, the "air pollution complex" (Zhu et al., 2023). The atmospheric oxidation capacity (AOC) determines the production rates of secondary pollutants in the atmosphere and is the essential driving force in forming complex air pollution (Z. Liu et al., 2021).

As a trace gaseous pollutant, nitrous acid (HONO) strongly impacts the AOC, the photolysis of which can contribute to more than 60 % of the OH radicals in the daytime (Czader et al., 2012). As an important source of OH radicals

in both rural and urban environments, HONO outweighs the contribution of ozone photolysis (Gu et al., 2022; Elshorbany et al., 2012; X. Yang et al., 2021). Thus, as an important source of oxidants for AOC, HONO can substantially influence the formation of secondary pollutants, exerting a considerable impact on air quality, climate change, and human health (Requia et al., 2018; Y. Zhang et al., 2021; Huang et al., 2018; Y. Liu et al., 2023).

Due to the importance of HONO for AOC, researchers have done lots of work on the transformation process of HONO, i.e., its sources and sinks. For the source of HONO, it is complicated and has been debated for decades. To sum it up, sources of atmospheric HONO mainly include the following:

a. *Direct emission from combustion, soil, and livestock farming*. The combustion includes vehicle exhaust, industrial exhaust, and biomass burning (Liao et al., 2021; Kurtenbach et al., 2001; Kirchstetter et al., 1996; Nie et al., 2015). The release from soil nitrite is one important primary source of HONO (Su et al., 2011; VandenBoer et al., 2015; Wu et al., 2019). The biological soil crusts can accelerate the HONO emission in drylands (Weber et al., 2015). Fertilization behavior of agricultural fields remarkably enhances the emission of HONO (Xue et al., 2021), and denitrification is one major HONO production pathway in boreal agricultural fields (Bhattarai et al., 2021). Meanwhile, livestock farming is also identified as an important primary emission source of HONO (Q. Zhang et al., 2023).

b. *Homogeneous reaction of OH + NO*. This is an important source of HONO. Although the reaction of OH+NO, which is the reverse reaction of HONO photolysis, does not contribute to an actual increase in free radicals, the assessment of this reaction pathway is significant for understanding the sources and sinks of HONO. Especially during the winter pollution period in the North China Plain, where there is usually a higher concentration of NO, this reaction pathway will contribute to a higher concentration of HONO (Xue et al., 2020).

c. *Heterogeneous conversion of NO_2 on various surfaces* (J. P. Liu et al., 2023; C. A. Yu et al., 2022; W. Yang et al., 2021). Finlayson-Pitts et al. (2003) reported that NO_2 could be converted to HONO on humid surfaces with first-order kinetics in NO_2. Xu et al. (2015) highlighted the HONO source had a large variability with heterogeneous conversion of NO_2 at ground face, and Aubin and Abbatt (2007) found that the heterogeneous conversion of NO_2 on hydrocarbon surfaces was an effective pathway to generate HONO.

d. *Photolysis of nitric acid and nitrate in particles in the daytime*. These were considered important sources of HONO in both experiments and field observations (Y. Wang et al., 2023; Ye et al., 2019; Yang et al., 2018; Ye et al., 2017). As for the sinks of HONO, diurnal photolysis is the main type of consumption (Keller-Rudek et al., 2013), and the reaction of HONO with OH radicals is also one sink that needs to be paid attention to (Cox et al., 1976).

Generally, HONO concentration in the atmosphere is closely related to the quality of the atmosphere. As heterogeneous processes are considered the main source of HONO, and most of which are poorly understood, many field observations of HONO were focused on haze-polluted environments (Li et al., 2012; Spataro et al., 2013; Tong et al., 2015; Xu et al., 2015; Hou et al., 2016). In urban areas, the HONO concentration can be as high as more than 10 ppb during severe pollution episode (W. Zhang et al., 2019). In China, the Chinese government has implemented series of stringent clean air actions to address the severe air pollution issue since 2013; significant reduction of $PM_{2.5}$ was observed in north and south China during 2013–2020 (Li et al., 2022). However, ozone levels have not been effectively reduced in China; the warm-season (from April to September) mean maximum daily 8 h average ozone (MDA8 O_3) increased by 2.6 $\mu g\,(m^{-3}\,yr^{-1})$ (Y. Liu et al., 2023). In view of the atmospheric changes in $PM_{2.5}$ and ozone, recent field observations have begun to pay attention to the potential influence of HONO on $PM_{2.5}$, ozone, and coexistence of $PM_{2.5}$ and ozone (W. Zhang et al., 2023; X. Zhang et al., 2023; Xuan et al., 2023; Chen et al., 2023; Zhang et al., 2022; Lin et al., 2022; Li et al., 2021). However, most HONO observations were conducted in autumn and winter, and the period was relatively short, usually a few weeks covering one or several pollution processes. Based on the increase in ozone in the warm season, long-term observations during the warm season are needed, yet they are rather limited.

In this work, we conducted one HONO observation in an urban site of Beijing; the time was from June to October 2021, covering the whole summer and part of autumn. According to the Technical Regulation for Ambient Air Quality Assessment (Trial), only 1 d of moderate pollution ($PM_{2.5}$, in October) and no more than 4 d of light pollution (ozone) per month were included, so we analyzed the observation data on a monthly basis. The atmospheric levels and variations of HONO and related species during each month were analyzed and compared. The impacts of HONO on atmospheric oxidant capacity in each month were also assessed.

2 Methods

2.1 Observation site and instruments

The observation campaign was conducted from 18 June to 25 October 2021. The observation site was located at the Chinese Research Academy of Environmental Sciences

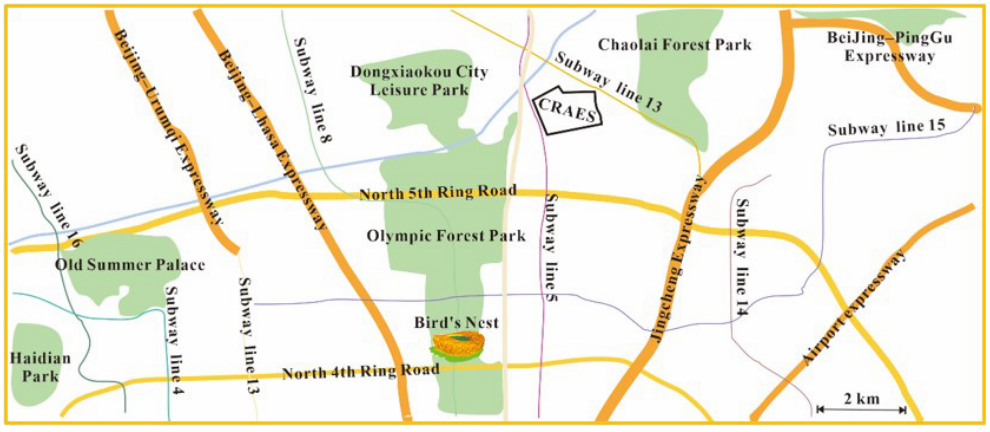

Figure 1. Location of the observation site in this work.

(CRAES; 40°04′ N, 116°42′ E), in the north of Chaoyang District, an urban site (Ren et al., 2022; X. Zhang et al., 2021) in Beijing, China (Fig. 1). Briefly, Chaoyang District is located at the eastern area of Beijing and is one of the six main urban districts (Dongcheng, Xicheng, Haidian, Chaoyang, Shijingshan, and Fengtai) of Beijing. This site is located about 2 km to the north of the North Fifth Ring Road, approximately 0.3 km away from Beiyuan Road, with a high volume of traffic. And this site was located in a mixed-use commercial and residential area, with several shopping malls, residential areas, and office buildings nearby, and there were no obvious sources of industrial pollution. Thus, this site could be considered an urban site.

HONO was measured with a water-based long-path absorption photometer (Chen et al., 2020), and the potential interferences, e.g., hydrolysis of NO_2, were subtracted by deploying a dual-channel absorption system. Briefly, the main structure of the instrument sampling unit is a double-channel stripping coil. In the first coil, almost all of the HONO and a small fraction of interfering species (e.g., NO_2, peroxyacetyl nitrate, NO_2^-) are absorbed by deionized water, while in the second channel, only a small fraction of interfering species is absorbed, which could be seen as the comparable conversion ratio in both the first and second channels. Therefore, the HONO concentration output by the instrument is the difference in concentration between the first and second channels. Concerning soluble species such as HO_2NO_2, considering its little ambient concentration, especially in the warm season, the interfering could be neglected (Veres et al., 2015). A set of commercial analyzers (Thermo 42i, 43i, 48i, 49i, 5030i, USA) were used to measure the concentrations of NO_x, SO_2, CO, O_3, and $PM_{2.5}$ online. Due to the employment of a molybdenum NO_2-to-NO converter, the 42i analyzer might overestimate NO_2 concentration for the potential conversion of NO_z ($NO_z = NO_y - NO_x$. e.g., HONO, HNO_3, and peroxyacetyl nitrate (PAN)). Based on this, we conducted field observations of NO_2 from 19 to 31 May 2024, using two devices with different measurement principles (Fig. S1 in the Supplement). The observation results showed that when the NO_2 concentration was above 7 ppb, there was no significant difference between the two devices. However, when it was below 7 ppb, the 42i values were significantly higher than those of the N500, with a corresponding slope of 1.14. Based on these data, we have adjusted all NO_2 values below 7 ppb during the observation period, as well as the corresponding analyses. The time resolution of the analyzers above was 1 min, and the detection limits were 0.4 ppbv, 0.5 ppbv, 0.04 ppmv, 1 ppbv, and 0.5 $\mu g\,m^{-3}$, respectively. In order to ensure the accuracy of the data, routine maintenance was carried out. The meteorological parameters (temperature, T; relative humidity, RH; pressure, P; and wind speed and direction, WS and WD) were obtained with an automatic weather station (MAWS301, Vaisala, Finland) with a time resolution of 1 h. Mass concentrations of the inorganic compositions in $PM_{2.5}$ (NO_3^-, SO_4^{2-}, Cl^-) were detected with a Monitor for AeRosols and Gases in ambient Air (MARGA; Model ADI 2080, Applikon Analytical B.V., the Netherlands) with 1 h resolution. Detailed descriptions of the instrument inlet design and the operating characteristics can be referred to in previous studies (Wang et al., 2022).

2.2 Photolysis rate simulation and OH estimation

Photolysis frequencies of JNO_2 were measured by a filter radiometer (METCON, Germany) with a time resolution of 1 min. Photolysis rate constants of O_3, HONO, and other parameters were simulated according to the aerosol optical depth and solar zenith angle by the Weather Research and Forecasting model coupled with Chemistry (WRF-Chem, version 3.7.1), based on the TUV model (http://cprm.acom.ucar.edu/Models/TUV/InteractiveTUV/, last access: 11 December 2023) (J. Zhang et al., 2019). To reduce the imprecision of model simulation, the observed JNO_2 value was used to correct simulated results, i.e., $J(O^1D)$ and J(HONO).

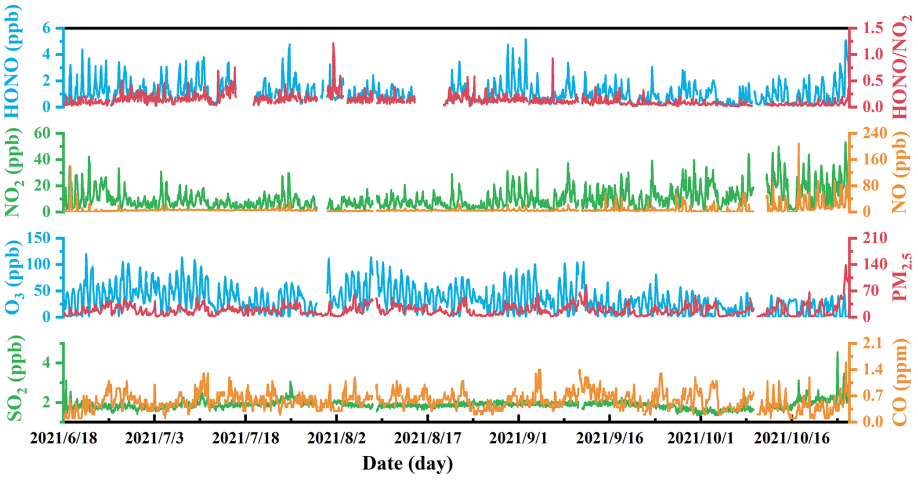

Figure 2. Temporal variations of hourly average $PM_{2.5}$, CO, O_3, SO_2, NO, HONO, NO_2, and $HONO/NO_2$ during the observation period.

The OH concentration was calculated with the following equation (Liu et al., 2019):

$$[\mathrm{OH}] = a \times \left(\frac{\mathrm{J(O^1D)}}{10^{-5}\,\mathrm{s^{-1}}} \right)^{b} + c, \quad (1)$$

where $a = 4.2 \times 10^6\,\mathrm{cm^{-3}}$, $b = 1$, and $c = 2.2 \times 10^5\,\mathrm{cm^{-3}}$ (Lin et al., 2022). These coefficients adopted here were from OH studies in the Pearl River Delta (PRD) and Beijing, China (Rohrer and Berresheim, 2006; Rohrer et al., 2014; Tan et al., 2017, 2018). The influence of the uncertainty of the coefficients was estimated (Liu et al., 2019). Results showed that the errors of OH increased with the increase in $J(O^1D)$, but the ratios of error to mean value of OH radicals were in an acceptable range of 0.37–0.55. According to the summarizing coefficients in different OH observation campaigns in the polluted areas of China (Liu et al., 2019), the comprehensive impact of reactants (e.g., volatile organic compounds (VOCs) and NO_x) on OH could not compete with that of UV light to OH; the chemical environments of OH could be similar. The OH concentration calculated through this formula was within a reasonable range and would not subvert the relative conclusions in this study. Thus, this could be a reasonable way to derive OH concentration by the equation above.

3 Results and discussion

3.1 Observation data overview

3.1.1 Variations of meteorological parameters during observation period

Figure S2 shows the time series of meteorological parameters including RH, T, WS, WD, and JNO_2 from 18 June to 25 October 2021. During the observations, the temperature ranged from 3.1–37 °C with an average of 23 °C, and the RH ranged from 7.1 %–100 % with an average of 59 %. The average wind speed during the observation was 1.1 $\mathrm{m\,s^{-1}}$, and the maximum wind speed was 5.20 $\mathrm{m\,s^{-1}}$. The average and monthly average values of T, RH, and WS are shown in Table S1 in the Supplement. As shown in Fig. S3 and Table S1, the temperature in June, July, and August was higher, 26–29 °C; temperature began to drop slightly in September, 22 °C; and in October, temperature dropped significantly, 13 °C. Meanwhile, the solar radiation in September and October decreased as the sun moved south. The maximum value of $J(NO_2)$ during the observation was $8.2 \times 10^{-3}\,\mathrm{s^{-1}}$, and the values reached a maximum at noon (with high solar radiation) and decreased to zero at night. The average wind speed also slightly decreased in September and October. During the observation, June had the lowest RH and the maximum wind speed, and due to the increase in precipitation, July had the highest RH. For the daily variation in meteorological parameters, T and JNO_2 expressed the same variation pattern with O_3, i.e., increasing after sunrise and decreasing after sunset, as shown in Fig. S3, while the RH showed the opposite pattern that was increasing during the night and decreasing during the daytime. For the WS, it was higher from 08:00 to 20:00 LT in June, and for the rest of the observation period, WS began to increase in the afternoon and subside after sunset.

3.1.2 Variations of pollutant species during observation period

Figure 2 shows the time series of basic parameters including HONO, NO_2, NO, CO, O_3, SO_2, PM_{10}, $PM_{2.5}$, and $HONO/NO_2$ from 18 June to 25 October 2021. The HONO concentration ranged from 0.05 to 5.2 ppb, with an averaged value of 1.1 ppb (the entire observation period). The concentration of O_3 ranged from 1 to 227 ppb, with an averaged value of 72 ppb (the entire observation period). The concentrations of NO_2, NO, CO, SO_2, and $PM_{2.5}$ were 0.56–53 ppb, 0.01–210 ppb, 0.1–1.6 ppm, 1.3–4.6 ppb, and

Table 1. The average and monthly average concentration of HONO, NO_2, NO, CO, O_3, SO_2, $PM_{2.5}$, HONO/NO_2, and HONO/NO_2 from June to October during the observation period.

Concentration		HONO (ppb)	NO_2 (ppb)	HONO/NO_2	NO (ppb)	CO (ppm)	O_3 (ppb)	SO_2 (ppb)	$PM_{2.5}$ ($\mu g\,m^{-3}$)
Average (the entire observation period)		1.1	10	0.052	7.9	0.56	72	1.9	19
June	average	1.3	12	0.051	5.7	0.52	88	1.8	20
	max	4.4	42	0.17	139	1.1	227	4	51
	min	0.14	2	0.0055	0.3	0.1	1	1.4	3
July	average	1.3	7.5	0.072	6.6	0.56	78	1.9	17
	max	4.8	31	0.54	29	1.3	211	3.1	53
	min	0.11	1.1	0.0061	2.2	0.1	1	1.5	1
August	average	1.0	7.1	0.079	4.8	0.57	87	1.9	19
	max	4.8	31	0.79	24	1.2	214	2.2	60
	min	0.052	0.62	0.0049	1.3	0.2	10	1.5	2
September	average	0.96	11	0.035	6.7	0.65	68	1.9	19
	max	5.2	40	0.19	57	1.4	210	2.3	86
	min	0.078	0.56	0.0042	0.39	0.2	9	1.3	1
October	average	0.89	17	0.025	17	0.46	40	1.9	23
	max	5.1	53	0.21	210	1.6	116	4.6	181
	min	0.066	1.7	0.0041	0.01	0.1	10	1.3	1

1–181 $\mu g\,m^{-3}$, respectively, with average values (the entire observation period) of 10 ppb, 7.9 ppb, 0.56 ppm, 1.9 ppb, and 19 $\mu g\,m^{-3}$, respectively. The average and monthly average concentrations of the basic parameters are shown in Table 1. One haze episode (1 d) occurred across the observation period, for which the daily mass concentration of $PM_{2.5}$ was 117 $\mu g\,m^{-3}$, higher than the National Ambient Air Quality Standard (Class II: 75 $\mu g\,m^{-3}$). And for O_3, eight episodes (13 d) occurred across the observation period, with MDA8 O_3 higher than Class II: 160 $\mu g\,m^{-3}$. Overall, the high HONO concentration was always accompanied by high concentration of NO_x (NO, NO_2) or aerosols ($PM_{2.5}$).

3.2 HONO observation comparison and pollution patterns

3.2.1 HONO observation comparison

For comprehensive comparative analysis, a review of the HONO observations in Beijing has been carried out in several recent years, and the results are shown in Table S2. Overall, the HONO measurement began to increase from 2016 in Beijing. The time was mainly concentrated in winter (December, January, and February), and most studies were pollution process analyses. In this work, the observation period was in summer and autumn. When the air quality was relatively poor in the early years, $PM_{2.5}$ and HONO concentrations were both relatively high. Now that the air quality of Beijing had improved, the concentration of both $PM_{2.5}$ and HONO decreased. However, during the observation period, $PM_{2.5}$ concentration was low, and HONO concentration was still relatively high compared with other results performed in summer. According to previous studies (Murthy et al., 2020; Du et al., 2013), the narrowing of the mixing layer could result in the accumulation of pollutants near the ground, while the increase in mixing layer height (MLH) favored the dilution of pollutants. In general, the MLH was low in winter and high in summer. And the photochemistry was quite active in summer because of the strong solar radiation; in this case, HONO tended to undergo photolysis. However, our observations showed that HONO concentration in summer was comparable to that in winter and spring and higher than that in autumn. J. Wang et al. (2023) also found that in the warm season, the $PM_{2.5}$ and MDA8 O_3 increased along with the development of MLH (MLH < 1200 m); they analyzed that the enhanced secondary chemical formation and increased atmospheric oxidant capacity could explain this phenomenon. Based on this, we discussed the HONO sources in the following sections.

3.2.2 HONO variation patterns

The average diurnal variation in the pollutants during the whole observation period and the averaged values in each month are shown in Figs. S4 and 3. It can be seen that the daily averaged pattern of pollutant HONO is that it decreased after sunrise and increased after sunset, and this variation pattern was similar to previous studies (Lin et al., 2022; Lian et al., 2022; J. Zhang et al., 2019, 2022; W. Zhang et

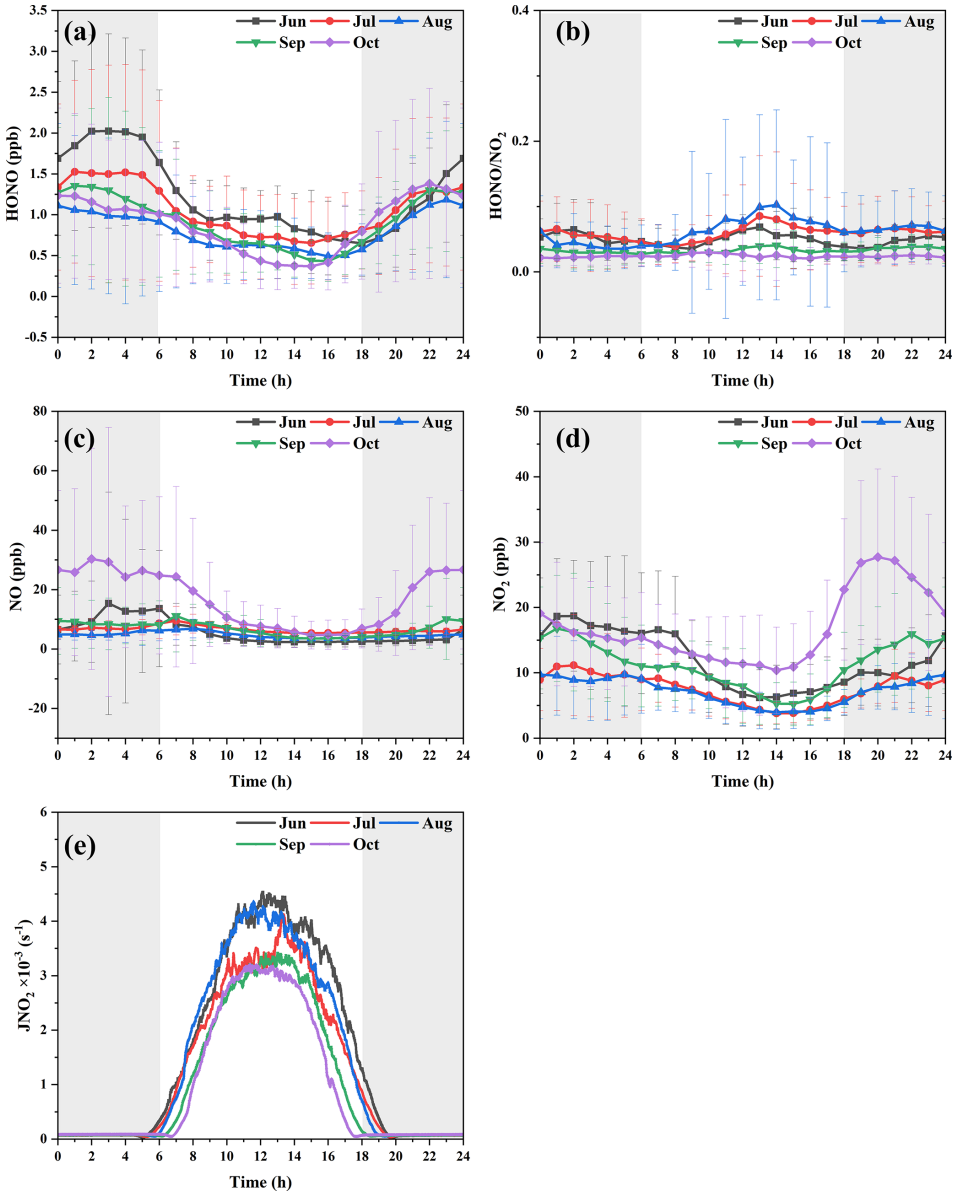

Figure 3. Diurnal variations in **(a)** HONO, **(b)** $HONO/NO_2$, **(c)** NO, **(d)** NO_2, and **(e)** JNO_2 in each month. The gray shading areas indicate nighttime, 18:00–06:00 LT.

Table 2. Emission ratios ($\Delta HONO/\Delta NO_x$) of fresh vehicle plumes.

Date	Time	$\Delta NO/\Delta NO_x$		$\Delta HONO/\Delta NO_x$	
		Slope (%)	R^2	Slope (%)	R^2
21 June 2021	02:25–03:15	99	1	2.5	0.73
31 August 2021	02:20–02:45	93	0.99	2.2	0.76
15 September 2023	03:30–04:20	104	0.98	2.1	0.83
22 September 2023	05:20–05:50	96	0.97	2.0	0.85
3 October 2023	00:40–00:55	94	0.99	1.2	0.93
8 October 2023	04:35–05:25	94	0.99	0.32	0.79

al., 2023). This trend was the same as NO_2, NO, $PM_{2.5}$, and CO; it was relatively stable overall, and it decreased slightly during the daytime. The diurnal variation in SO_2 was not large, and the overall concentration was very low, but it had a slight increase during the daytime. The variation in O_3 showed the opposite trend; i.e., its concentration increased after sunrise, peaked in the afternoon, and decreased at night. The rapid decrease in HONO in the daytime was caused by rapid photolysis and the increase in boundary layer height. The ratio of $HONO/NO_2$ is often used to characterize the heterogeneous reaction of NO_2 to form HONO (W. Yang et al., 2021; El Zein et al., 2013; Romanias et al., 2012). At night, the $HONO/NO_2$ ratio was similar to that of HONO, but the ratio increased obviously during the daytime, especially in summer (June, July, August), and in summer, the light intensity was very strong, as revealed in Fig. 3b and e. This phenomenon indicated that HONO might have other potential sources related to the solar radiation, e.g., the conversion of NO_2 to HONO or nitrate photolysis.

And when HONO was analyzed in months, the characteristics of each month were different. For the $HONO/NO_2$ ratio in Fig. 3b, August, July, June, and September were the months with a significant increase in the noon period, and there was no such phenomenon in October. However, it was important to note that the NO and NO_2 concentrations in October were the highest in the entire observation period compared to the low HONO concentration. The NO and NO_2 concentrations in June were not high, but the HONO concentration was the highest. The phenomenon could not be explained by the well-known sources of HONO (Xuan et al., 2023).

3.3 Nocturnal HONO sources and formation

3.3.1 Direct emission of HONO

Previous studies showed that the primary emission sources of HONO included biomass burning and vehicles as well as soil emissions (Nie et al., 2015; Su et al., 2011). In this study, soil emission was a negligible source of HONO, since the observation site was located in an urban area, and the surrounding soil was not used for agriculture, which greatly reduced HONO emission caused by fertilization process (Su et al., 2011). Except organic compounds (Simoneit, 2002), CO in the gas phase (Andreae, 2019) and potassium ions (K^+) in the aerosol phase (Xinghua et al., 2007) were well-recognized inorganic tracers of biomass burning. Many CO sources other than biomass burning, such as industry and traffic, could contribute significantly to the CO loading. Apart from biomass burning emissions, there were no other significant sources of K^+ during the measurement. Therefore, K^+ was a suitable tracer of biomass burning. According to studies on the influence of biomass burning on HONO chemistry (Nie et al., 2015), when K^+ concentration is higher than $2\,\mu g\,m^{-3}$ and the ratio of K^+ to $PM_{2.5}$ is larger than 0.02, the plumes are defined as biomass burning samples, while the samples with K^+ concentrations lower than $2\,\mu g\,m^{-3}$ and a ratio of K^+ to $PM_{2.5}$ smaller than 0.02 are categorized as non-biomass burning samples. The average K^+ levels during the 5 months were 0.14, 0.11, 0.11, 0.15, and $0.13\,\mu g\,m^{-3}$, respectively, lower than $2\,\mu g\,m^{-3}$ (Nie et al., 2015), which indicated that biomass burning had little effect on this observation site. Hence, only vehicle emission was considered in this study.

The $HONO/NO_x$ ratio was used to derive the emission factor of vehicles in fresh plumes (Kurtenbach et al., 2001). Criteria followed by the fresh plumes were as follows (Yun et al., 2017):

a. $\Delta NO/\Delta NO_x > 0.9$,

b. good correlation between NO_x and HONO ($R^2 > 0.7$),

c. short duration of plumes < 1 h,

d. positive correlation between CO and NO_x,

e. no precipitation,

f. global radiation $< 10\,W\,m^{-2}$ or $JNO_2 < 0.25 \times 10^{-3}\,s^{-1}$.

A total of six cases met the criteria mentioned above, and the details are summarized in Table 2. The mean $\Delta NO/\Delta NO_x$ ratio of the selected fresh plumes was $(97 \pm 4.4)\,\%$, which indicated that the chosen air masses were considered to be truly fresh. The linear slope of HONO with NO_x was used as the emission factors of HONO. The correlation coefficients (R^2) between HONO and NO_x varied among the cases due to the unavoidable mixing with other air masses, and the range was from 0.72 to 0.93. The obtained $\Delta HONO/\Delta NO_x$ ratios were from 0.32 % to 2.49 %, with an average value of $(1.7 \pm 0.74)\,\%$. Thus, a mean $\Delta HONO/\Delta NO_x$ value of 0.017 was used as the emission factor (EF) in this work. The $\Delta HONO/\Delta NO_x$ values obtained in an urban area of Beijing in previous studies are also summarized in Table S2. The EF reported so far has been concentrated in the range of 0.003–0.013, which is slightly lower than the EF in this work. The vehicle engine types, catalytic converter use, and fuels could affect the emission factors of vehicles (Kurtenbach et al., 2001). According to Kessler and Platt (1984), diesel engines had a higher $HONO/NO_x$ ratio than gasoline engines. In our study, the higher $HONO/NO_x$ value was possibly due to the observation site being located outside the Fifth Ring Road and more heavy-duty diesel vehicles passing by on the surrounding road at night (regulations of the Public Security Traffic Management Bureau of the Beijing Municipal Public Security Bureau, i.e., from 06:00 to 23:00 LT). Every day, trucks are prohibited from passing on the roads within the Fifth Ring Road (exclusive), and trucks with an approved load weight of more than 8 t (inclusive) are prohibited on the main road

Table 3. The conversion frequency k_{HONO} and $k_{HONO}[NO_2]$ in each month during the observation period.

	June	July	August	September	October
$k_{HONO,het\text{-}night}$ (h^{-1})	0.011 ± 0.003	0.01 ± 0.002	0.0093 ± 0.0015	0.0081 ± 0.0006	0.0016 ± 0.0002
$k_{HONO,het\text{-}night}[NO_2]$ (ppb h^{-1})	0.15 ± 0.02	$0.089 \pm 0.6\,\%$	$0.079 \pm 0.004\,\%$	0.11 ± 0.01	0.032 ± 0.001

of the Fifth Ring Road. Assuming that NO_x mainly arose from vehicle emissions, the mean $\Delta HONO/\Delta NO_x$ value of 0.017 was adopted to estimate the vehicle emissions P_{emis} (ppb h^{-1}) contribution to the HONO concentration (this factor may lead to an overestimation of the P_{emis} in the daytime):

$$P_{emis} = NO_x \times EF. \quad (2)$$

Then, the concentration of HONO in air that is not due to direct vehicular emissions (the corrected HONO concentration, $HONO_{corr}$) can be obtained from the following equation:

$$HONO_{corr} = HONO - P_{emis}. \quad (3)$$

3.3.2 Nighttime heterogeneous conversion of NO_2

Heterogeneous conversion of NO_2 on the ground or the aerosol surface has been recognized as an important HONO source (Finlayson-Pitts et al., 2003; Liu et al., 2020). Nighttime $HONO_{het\text{-}night}$ concentration could be estimated from the heterogeneous reaction (Reaction R1, the mechanism of heterogeneous formation of HONO), and this was with first-order kinetics in NO_2 and H_2O (Alicke, 2002), and the conversion frequency of HONO ($k_{HONO,het\text{-}night}$) could be expressed as Eq. (6). We determined the HONO formation by assuming a linear increase in its mixing ratio during a time interval ($t_2 - t_1$). Since the mechanism summarized in Reaction (R1) was with first-order kinetics in NO_2, the HONO formation was proportional to the NO_2 concentration. The conversion frequency was also assumed to be independent of gas-phase water (Kleffmann et al., 1998). The average nighttime conversion frequency was determined by Eqs. (4)–(6). In order to eliminate the influence of direct emission and diffusion, CO was chosen as the reference species used for normalization:

$$2NO_2 + H_2O \xrightarrow{\text{ground, aerosol surface}} HONO + HNO_3 \quad (R1)$$

$$k^0_{HONO} = \frac{[HONO_{corr,night}]_{t2} - [HONO_{corr,night}]_{t1}}{(t_2 - t_1)\overline{[NO_2]}} \quad (4)$$

$$k^X_{HONO} = \frac{\left(\frac{[HONO_{corr,night}]_{t2}}{[X]_{t2}} - \frac{[HONO_{corr,night}]_{t1}}{X_{t1}}\right)\overline{[X]}}{0.5(t_2 - t_1)\left(\frac{[NO_2]_{t2}}{[X]_{t2}} + \frac{[NO_2]_{t1}}{[X]_{t1}}\right)\overline{[X]}} = \frac{2\left(\frac{[HONO_{corr,night}]_{t2}}{[X]_{t2}} - \frac{[HONO_{corr},night]_{t1}}{X_{t1}}\right)}{(t_2 - t_1)\left(\frac{[NO_2]_{t2}}{[X]_{t2}} + \frac{[NO_2]_{t1}}{[X]_{t1}}\right)} \quad (5)$$

$$k_{HONO,het\text{-}night} = \frac{1}{2}\left(k^0_{HONO} + k^{CO}_{HONO}\right), \quad (6)$$

where $\overline{[NO_2]}$ was the mean value of NO_2 concentration between time t_2 and t_1, k^0_{HONO} was the conversion frequency which was not scaled, and k^X_{HONO} was the conversion frequency scaled with reference gases X (CO). Then, the NO_2/HONO conversion rate (k_{HONO}) was calculated by the combination of k^0_{HONO} (not scaled k_{HONO}) and k^{CO}_{HONO} (CO scaled k_{HONO}), which could reduce the impact of uncertainties in diffusion process and emissions on the conversion rate.

The averaged values of $k_{HONO,het\text{-}night}$ during the observation period were $0.011\,h^{-1}$, $0.01\,h^{-1}$, $0.0093\,\%\,h^{-1}$, $0.0081\,h^{-1}$, and $0.0016\,h^{-1}$, respectively, for June, July, August, September, and October, with $0.008\,h^{-1}$ on average. The averaged value was slightly higher than that reported by Xuan et al. (2023) and Jia et al. (2020), 0.0073 and $0.0078\,h^{-1}$ from August to September 2018. The varied values of k_{HONO} in each month indicated the different environmental conditions in each month, e.g., surface features and aerosol concentrations (Su et al., 2008). As shown in Table 3, June had the highest $k_{HONO,het\text{-}night}[NO_2]$; this indicates that the heterogeneous conversion from NO_2 was more important for HONO formation at night in June.

In general, the importance of the two generation pathways of nocturnal HONO might change due to the time and environmental factors. North China has four distinct seasons, and temperature and relative humidity vary with the seasons. Pollutants in the gas phase and particle phase in the environment can also be affected, and the factors of observation location and observation time should be taken into account when evaluating the relative contribution of the generation pathways to HONO.

3.4 HONO daytime budget

3.4.1 Budget analysis of HONO

According to the source and sink pathways of HONO mentioned in the Introduction, the sources of HONO in the daytime (10:00–15:00 LT) include the following: (1) direct emission of HONO (P_{emis}), (2) homogeneous reaction of NO with OH ($P_{OH+NO} = k_{OH+NO}[OH][NO]$), (3) unknown sources during the daytime ($P_{unknown}$), and (4) the vertical (T_v) and horizontal (T_h) transport processes of HONO. According to related observations (Wong et al., 2011, 2012, 2013; Pinto et al., 2014; Stutz et al., 2002; Wang et al., 2006; VandenBoer et al., 2013; Young et al., 2012), photolytic HONO formation on the ground is the major formation pathway in the lowest 20 m, while a combination of gas-phase, photolytic formation on aerosol and vertical transport is responsible for daytime HONO between 200 and 300 m above the ground. In our work, the measurement was conducted on the rooftop of one building, about 8 m above the ground. Vertical exchange is unknown since the data to calculate its effect on HONO measured at 8 m are not available. Therefore, all subsequent analysis relies on the assumption that vertical exchange is unimportant, but this assumption represents an uncertainty that is not easily quantified; the sinks of HONO on the daytime include the following: (1) dry deposition of HONO ($L_{dep} = \frac{V_{HONO}}{H}[HONO]$), (2) photolysis of HONO ($L_{phot} = J_{HONO}[HONO]$), and (3) reaction of OH with HONO ($L_{OH+HONO} = k_{OH+HONO}[HONO][OH]$).

The budget of HONO can be calculated by the following equations:

$$\frac{dHONO}{dt} = (P_{emis} + P_{OH+NO} + P_{unknown}) - (L_{dep} + L_{phot} + L_{OH+HONO}) \quad (7)$$

$$P_{unknown} = \frac{dHONO}{dt} + L_{dep} + L_{phot} + L_{OH+HONO} - P_{emis} - P_{OH+NO} \quad (8)$$

$$P_{unknown} = \frac{\Delta HONO}{\Delta t} + k_{OH+HONO}[OH][HONO] + J_{HONO}[HONO] + \frac{V_{HONO}}{H}[HONO] - k_{OH+NO}[OH][NO] - P_{emis}, \quad (9)$$

where $\frac{dHONO}{dt}$ represents the difference between HONO sources and sinks; $\frac{\Delta HONO}{\Delta t}$ was the observed change of HONO; and the rate constants of k_{NO+OH} and $k_{HONO+OH}$ at 298 k were 9.8×10^{-12} and 6.0×10^{-12} cm^3 $molec.^{-1}$ s^{-1}, respectively (J. Liu et al., 2021). A value of $V_{HONO} = 1.6$ cm s^{-1} was adopted here for the deposition rate of HONO (W. Zhang et al., 2019). A value of $H = 200$ m was used here as the mixing layer height (Hu et al., 2022). The OH concentration and J_{HONO} were calculated using the method mentioned in Sect. 2.2. According to the model simulation results, the averaged J_{HONO} values were in the range of 0.78×10^{-3}–1.4×10^{-3} s^{-1}. The daytime hourly averaged values of OH concentration in the 5 months were in the range of 2.9×10^6–8.9×10^6 molec. cm^{-3}.

Figure 4 illustrates the details of the production and loss rates and proportion of HONO during the observation period. Table S3 shows the averaged production and loss rates of HONO around noontime (10:00–15:00 LT). The dominant loss pathway of HONO during the 5 months was the photodecomposition (L_{phot}), of which the averaged values of L_{phot} were 1.1–3.9 ppb h^{-1} around noontime. The following loss pathway of HONO was dry deposition (L_{dep}), of which the averaged values of L_{dep} were 0.13–0.27 ppb h^{-1} around noontime. The loss pathway with the least contribution was the reaction of OH with HONO ($L_{OH+HONO}$), of which the averaged values of $L_{OH+HONO}$ were 0.029–0.15 ppb h^{-1} at the same time. For the production pathways of HONO around noontime, the averaged values of homogeneous reaction rate between NO and OH (P_{OH+NO}) were 0.64–1.5 ppb h^{-1}. The averaged values of P_{emis} were 0.16–0.33 ppb h^{-1}. For the high value of P_{emis} in October, the possible reasons may be that the corresponding diffusion conditions were weakened due to the decrease in wind speed, and the change of epidemic control policies in this area in October resulted in the increase in the traffic emissions. The averaged values of $P_{unknown}$ were 0.29–2.7 ppb h^{-1}, the contribution of which to the production of HONO were 78 % (June), 55 % (July), 64 % (August), 68 % (September), and 30 % (October), respectively. In summary, photodecomposition was the largest removal pathway around noontime during the whole observation period. $P_{unknown}$ contributed the most to the production of HONO in June, July, August, and September. Homogeneous reaction of NO and OH dominated the HONO production in October in the daytime. June had the highest $P_{unknown}$, and October had the lowest $P_{unknown}$.

The obtained average $P_{unknown}$ value in summer (from June to August), 2.3 ppb h^{-1}, was at the middle level of the levels reported in literature studies in urban areas, as shown in Table 4. The $P_{unknown}$ value in autumn (from September to October) (1.0 ppb h^{-1}) was at the lower–middle level of those reported in literature studies in urban areas.

3.4.2 Possible unknown source in the daytime

Based on the assumption that nighttime heterogeneous conversion of NO_2 continued in the same way at the daytime, the nighttime heterogeneous production of HONO was adopted here, and $P_{het} = k_{HONO}[NO_2]$ (Alicke, 2002; Sörgel et al., 2011). Dark heterogeneous formation accounted for 6.5 % (June), 4.9 % (July), 2.9 % (August), 6.5 % (September), and 11 % (October) of missing sources of HONO in the daytime, respectively, which was almost negligible in the daytime. And the average value of $P_{unknown}$ normalized by NO_2 in the daytime (10:00–15:00 LT) was 0.025–0.61 h^{-1}, as shown in

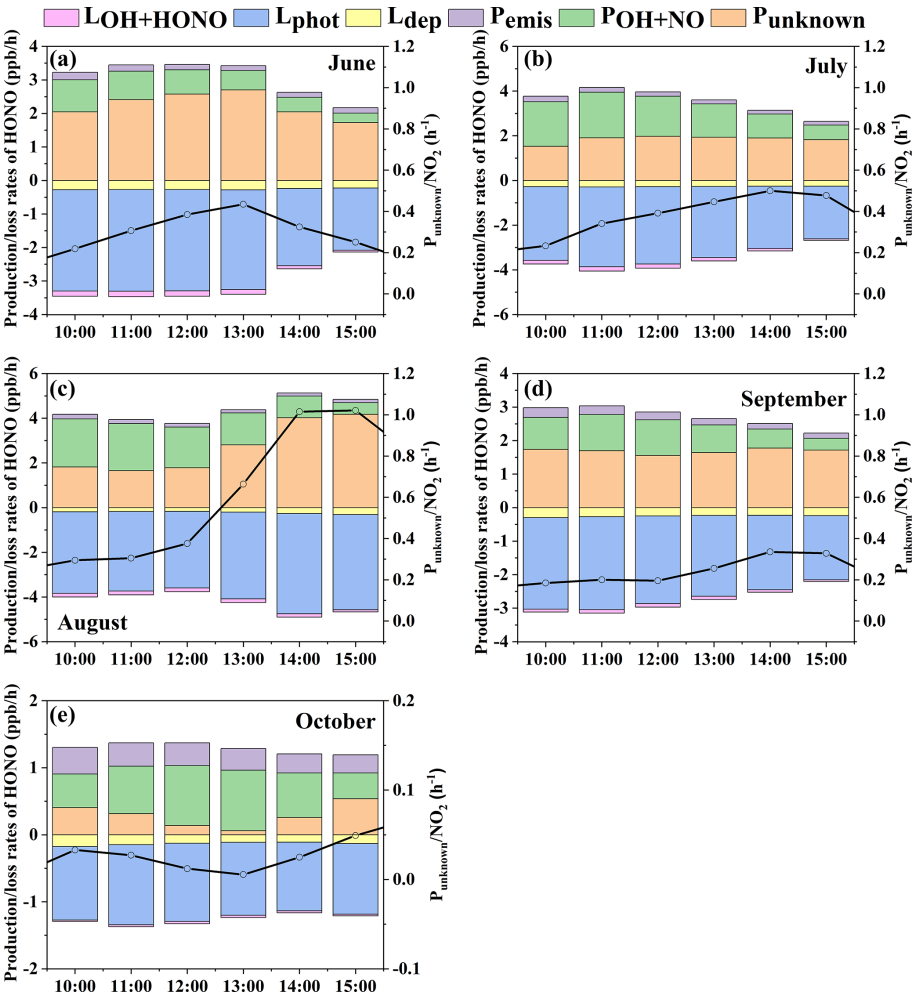

Figure 4. Daytime HONO budget in average production (P_{emis}, P_{NO+OH}, $P_{unknown}$) and loss rates ($L_{OH+HONO}$, L_{phot}, L_{dep}) during the 5 months.

Table 4. The $P_{unknown}$ values in this work and reported in literature studies.

	Date	Value (ppb h^{-1})	Location	Literature study
Summer	18 August to 16 September 2018	0.49	Beijing	Xuan et al. (2023)
	June to July 2019	0.59	Beijing	Li et al. (2021)
	24 July to 6 August 2015	0.75	Xi'an	Huang et al. (2017)
	1 June to 31 August 2018	0.98	Nanjing	Liu et al. (2019)
	8–20 March 2005	1.7	Santiago	Elshorbany et al. (2009)
	June to August 2021	2.3	Beijing	This work
	25 May to 15 July 2018	2.1	Beijing	J. Liu et al. (2021)
	1 June to 31 August 2016	3.0	Jinan	Li et al. (2018)
	20 June to 25 July 2016	3.8	Beijing	J. Wang et al. (2017)
	August 2018	4.5	Xiamen	Hu et al. (2022)
Autumn	27 September to 9 November 2018	0.65	Guangzhou	Y. Yu et al. (2022)
	September to October 2021	1.1	Beijing	This work
	October 2018	2.1	Xiamen	Hu et al. (2022)
	23 August to 17 September 2018	2.3	Beijing	Jia et al. (2020)
	22 September to 21 October 2015	3.1	Beijing	J. Wang et al. (2017)

Table S3, much greater than the conversion rates in the nighttime. This phenomenon implied that $P_{unknown}$ could not be explained by the nocturnal mechanism of NO_2 to HONO.

According to the possible HONO sources reported in literature studies (X. Zhang et al., 2023; Zhang et al., 2022; Lian et al., 2022), light-induced heterogeneous conversion from NO_2 to HONO and photolysis of nitrate were responsible for $P_{unknown}$, and solar illumination and relative humidity were the two most frequently considered meteorological factors. Thus, a correlation analysis was performed to explore the potential unknown sources of HONO in the daytime, and the details are shown in Table S4.

J. Wang et al. (2017) analyzed the data of Beijing from 20 June to 25 July 2016 (summer) and found that, compared to JNO_2 or RH alone, the correlation between $P_{unknown}$ and products of JNO_2 and RH was good. Based on this phenomenon, it was thought that photolytic and heterogeneous reactions occurring upon wet surfaces were important unknown sources of HONO. In our work, good correlation between $P_{unknown}$ and product of JNO_2 and RH was found in June. However, this phenomenon was not evident in the other 4 months. The phenomenon was not evident in 4 of the 5 months; this showed that in this observation there was not strong evidence for this conclusion. As shown in Table S4, June had the lowest RH and the highest JNO_2 value. The other 4 months had relative higher RH (due to the precipitation) and lower JNO_2 values. This phenomenon may be closely related to meteorological conditions and requires further research for validation.

In August and September, it could be seen that low NO_2 and $PM_{2.5}$ conditions could lead to high $P_{unknown}$, corresponding to high JNO_2 values and relatively low RH (20 %–40 %). This phenomenon suggested that there were other possible unknown sources of HONO, and this might be due to the light-enhancing effect of NO_2 on non-aerosol surfaces.

Through heterogeneous photochemical simulation experiments, Wingen et al. (2008) found that an enhanced NO_2 yield was observed as the chloride to nitrate ratio increased. Jin et al. (2022) performed nitrate photolysis experiments with a flow tube reactor and found that surprising yields of HONO and NO were formed during the photolysis experiment of NH_4NO_3 in the presence of halogen ions (Cl^-, Br^-, I^-); this phenomenon indicated the important role of halogen ions in the nitrate photolysis process. Thus, we analyzed the correlation between nitrate and $P_{unknown}$ in the presence of Cl^- ions. As shown in Table S4, the correlation between $P_{unknown}$ and the corresponding factors was as follows: $JNO_2 \times [NO_3^-] \times Cl^-$ ($R = 0.46$, $P < 0.05$) > $JNO_2 \times [NO_3^-]$ ($R = 0.29$, $P < 0.05$) in July; $JNO_2 \times [NO_3^-] \times RH \times Cl^-$ ($R = 0.44$, $P < 0.05$) > $JNO_2 \times [NO_3^-] \times RH$ ($R = 0.30$, $P < 0.05$) in July. Bao et al. (2018) found that large amounts of HONO and NO_x were formed during the photolysis experiment of nitrate in the presence of sulfate. Significant positive correlations also occurred in our observations in July: $JNO_2 \times [NO_3^-] \times SO_4^{2-}$ ($R = 0.32$, $P < 0.05$) > $JNO_2 \times [NO_3^-]$ ($R = 0.29$, $P < 0.05$); $JNO_2 \times [NO_3^-] \times RH \times SO_4^{2-}$ ($R = 0.33$, $P < 0.05$) > $JNO_2 \times [NO_3^-] \times RH$ ($R = 0.30$, $P < 0.05$). Yang et al. (2018) and Ye et al. (2019) found that the presence of organic components significantly enhanced the denitrification rate of nitrate. In this work, organic carbon (OC) was used as a proxy for organic components, and the correlation was analyzed. As shown in Table S4, the enhancement of the correlation between $P_{unknown}$ and NO_3^- in the presence of OC was observed, $JNO_2 \times [NO_3^-] \times OC$ ($R = 0.55$, $P < 0.05$) > $JNO_2 \times [NO_3^-]$ ($R = 0.48$, $P < 0.05$) in June. However, the phenomenon above was not evident in 4 of the 5 months. This shows that in this observation there was not strong evidence for these conclusions but that they could contribute based on the prior literature.

3.4.3 OH production rate in the daytime

As HONO was the efficient source of OH radical in the daytime (X. Zhang et al., 2023; Y. Yu et al., 2022), the OH production rate from HONO ($P_{OH-HONO}$) at the CRAES observation site was calculated in this work. The formaldehyde was not measured in this work, which was a large and known HO_x source in urban areas; thus the analysis here was not a full HO_x budget.

Figure 5 shows that the OH production rate from HONO usually occurred before noontime, and this was caused by the existing HONO and its photolysis. This phenomenon was obvious in July, September, and October. And for P_{OH-O_3} (the production rate of OH radical via O_3 photolysis to O1D followed by reaction with water vapor), the highest value was around noontime, which coincided with the $J(O^1D)$ trend. This phenomenon was obvious in June, July, and August. In September and October (autumn), the highest value of P_{OH-O_3} occurred a little later after noontime. The average $P_{OH-HONO}$ during 08:00–16:00 LT was 2.7 ppb h^{-1} (June), 2.9 ppb h^{-1} (July), 2.0 ppb h^{-1} (August), 2.3 ppb h^{-1} (September), and 0.93 ppb h^{-1} (October), respectively, and the average P_{OH-O_3} during 08:00–16:00 LT was 0.45 ppb h^{-1} (June), 0.82 ppb h^{-1} (July), 0.51 ppb h^{-1} (August), 0.33 ppb h^{-1} (September), and 0.048 ppb h^{-1} (October), respectively; the contribution of HONO to OH was significantly greater than that of ozone. The important role of HONO to OH in the atmospheric oxidizing capacity should benefit the production of photochemical ozone (Xuan et al., 2023; Jia et al., 2023; Zhang et al., 2022; W. Zhang et al., 2023), the formation of new particles (Stolzenburg et al., 2023), and the formation of secondary aerosols (X. Zhang et al., 2023; Xuan et al., 2023; J. Liu et al., 2021).

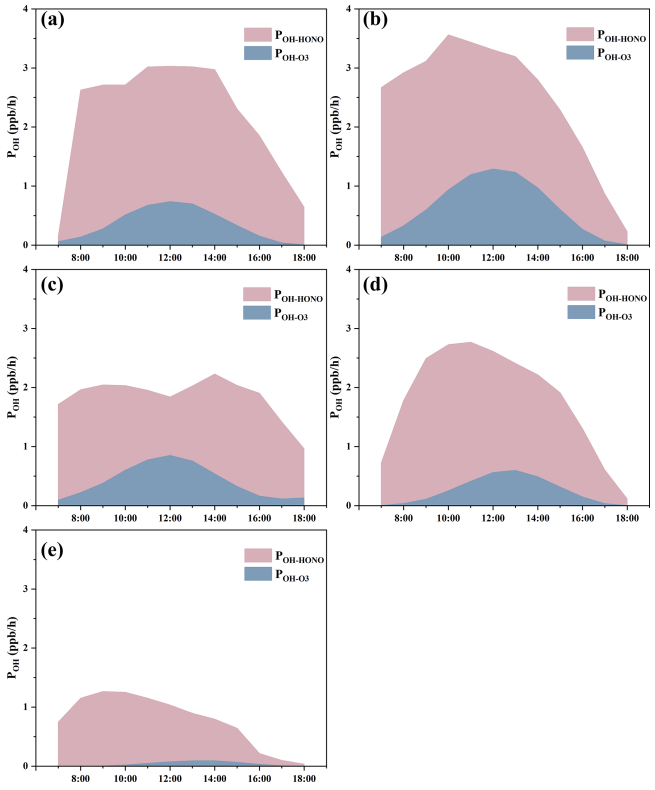

Figure 5. Averaged OH production rates from photolysis of HONO and ozone in **(a)** June, **(b)** July, **(c)** August, **(d)** September, and **(d)** October.

3.5 The correlations between HONO, $PM_{2.5}$, and O_3

In view of the importance of HONO for the atmospheric oxidizing capacity (Zhong et al., 2023; W. Zhang et al., 2023; Song et al., 2023), the correlations between HONO, $PM_{2.5}$, and O_3 were analyzed. According to the Technical Regulation on Ambient Air Quality Index (trial) in China (633—2012, 2012), $PM_{2.5}$ concentrations were divided into three zones, ≤ 35, 35–75, and $\geq 75\,\mu g\,m^{-3}$, and analyzed in the nighttime and daytime, respectively.

As shown in Fig. 6, $PM_{2.5}$ concentrations were positively correlated with HONO; i.e., the increase in $PM_{2.5}$ pollution was accompanied by the increase in HONO concentration during the daytime. At night, except in September, the same pattern was presented. One possible explanation of this phenomenon was that the increase in particle pollution in summer and autumn might lead to the formation of HONO and an increase in its concentration. Another possible explanation was that high HONO concentrations could lead to higher oxidative capacity and therefore higher rates of aerosol formation. There was also a possible explanation as both $PM_{2.5}$ and HONO stemmed from the same sources (i.e., their concentrations would both increase during pollution events). However, when it came to ozone, we could see a different phenomenon. In June and July, ozone showed a decreasing trend as particle and HONO concentrations increased during the daytime, but at night, ozone concentrations tended to increase. In August and September, ozone showed an increasing trend as particle and HONO concentration increased during both the daytime and nighttime. In October, ozone showed an increasing trend in the daytime but a decreasing trend at night. T. Wang et al. (2017) summarized ozone abundance and its relationship to chemical processes and atmospheric dynamics in China, reporting that ozone formation and concentration could be affected by various factors, including precursors, meteorological factors, and regional transport. The formation of OH radicals by HONO photolysis was a pathway involved in the RO_x and NO_x cycle of ozone formation; ozone was not directly related to HONO.

J. Wang et al. (2023) analyzed the relationships between ozone, $PM_{2.5}$, and mixing layer height in the warm season and found that the enhanced atmospheric oxidant capacity could promote the secondary transformation of particles and weaken the dilution effect of mixing layer height rise on pollutants. The contribution of observed HONO to the atmospheric oxidant capacity exceeded that of ozone, so it was necessary to pay more attention to the sources of HONO in the warm season.

4 Conclusions

Continuous field observation of HONO in the warm season was conducted in an urban site of Beijing, from June to October 2021. The monthly average HONO concentration was in the range of 0.89–1.28 ppb, showing a larger contribution to OH radical relative to ozone in the daytime, 3 times more than that of ozone each month. Compared with previous field observations in the urban sites of Beijing, the contribution of vehicle emissions to HONO (0.017) was relatively high. The monthly nocturnal conversion rate of $HONO/NO_2$ was in the range of 0.0016–0.011 h^{-1}, accounting for 2.9 %–11 % of missing sources of HONO in the daytime; the average value of $P_{unknown}$ normalized by NO_2 in the daytime (10:00–15:00 LT) was 0.025–0.61 h^{-1}, much greater than the conversion rates in the nighttime, which indicated that nocturnal heterogeneous conversion from NO_2 to HONO was almost negligible in the daytime.

Based on the field observations in summer and winter, Z. Liu et al. (2021) evaluated the atmospheric oxidizing capacity in the megacity of Beijing and found that the atmospheric oxidizing capacity showed a clear seasonal pattern, which was stronger in summer than in winter. The dominant oxidant contributor to the atmospheric oxidizing capacity in the daytime was the OH radical, and ozone was the second-most-important oxidant. Our work showed that in summer and autumn, the contribution of HONO to OH radicals was significantly greater than that of ozone; this further illustrated the importance of HONO. As mentioned in Sect. 3.4.1, the contributions of $P_{unknown}$ to the production of HONO were

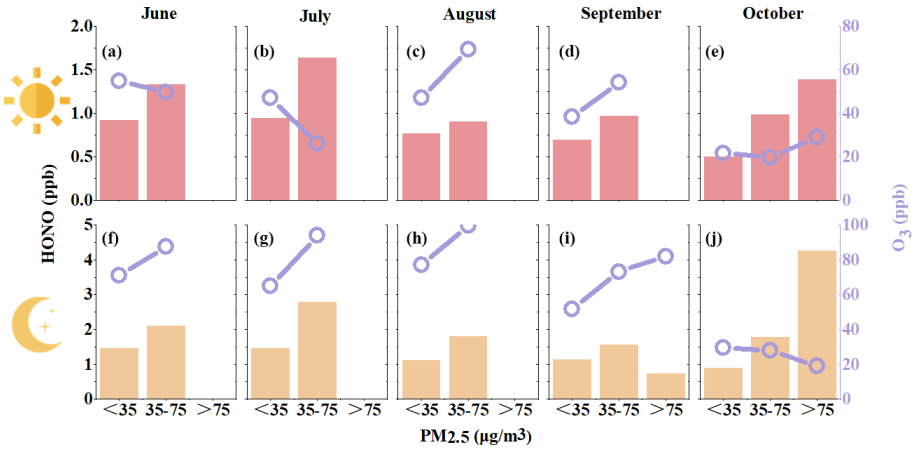

Figure 6. Distributions of HONO and O_3 mean concentrations under different $PM_{2.5}$ pollution conditions. The upper panel is the daytime average value (07:00–18:00 LT), and the bottom panel is the nighttime average value (19:00–06:00 LT).

78 % (June), 55 % (July), 64 % (August), 68 % (September), and 30 % (October), respectively. According to the OH production from HONO, the OH production rate from the missing HONO was also very important to the atmospheric oxidation capacity. Thus, further investigation was required to figure out the source of HONO. In recent years, the concentration of atmospheric particulate matter in China has decreased significantly, but the ozone concentration has shown a fluctuating upward trend, and the atmospheric oxidation capacity has increased significantly, especially in the warm season. Given the contribution of HONO to the atmospheric oxidation capacity, its sources should be studied in more detail.

Data availability. The data used in this study are available upon request from the corresponding author.

Supplement. The supplement related to this article is available online at https://doi.org/10.5194/acp-25-2551-2025-supplement.

Author contributions. JLL and HL conceived and led the studies. JLL, CFL, HZ, WGW, and HL performed observation studies and data analysis. MML, YXY, YFS, CC, YCG, YSX, JG, and MFG discussed the results and commented on the paper. JLL prepared the article with contributions from all co-authors.

Competing interests. The contact author has declared that none of the authors has any competing interests.

Disclaimer. Publisher's note: Copernicus Publications remains neutral with regard to jurisdictional claims made in the text, published maps, institutional affiliations, or any other geographical representation in this paper. While Copernicus Publications makes every effort to include appropriate place names, the final responsibility lies with the authors.

Financial support. This research has been supported by the National Key Research and Development Program of China (grant no. 2023YFC3706102) and the National Natural Science Foundation of China (grant nos. 41931287, 42130606, 42175133, and 42307139).

Review statement. This paper was edited by Steven Brown and reviewed by James Roberts and two anonymous referees.

References

Alicke, B.: Impact of nitrous acid photolysis on the total hydroxyl radical budget during the Limitation of Oxidant Production/Pianura Padana Produzione di Ozono study in Milan, J. Geophys. Res., 107, 8196, https://doi.org/10.1029/2000jd000075, 2002.

Andreae, M. O.: Emission of trace gases and aerosols from biomass burning – an updated assessment, Atmos. Chem. Phys., 19, 8523–8546, https://doi.org/10.5194/acp-19-8523-2019, 2019.

Aubin, D. G. and Abbatt, J. P. D.: Interaction of NO_2 with hydrocarbon soot: Focus on HONO yield, surface modification, and mechanism, J. Phys. Chem. A, 111, 6263–6273, https://doi.org/10.1021/jp068884h, 2007.

Bao, F. X., Li, M., Zhang, Y., Chen, C. C., and Zhao, J. C.: Photochemical aging of Beijing urban $PM_{2.5}$: HONO production, Environ. Sci. Technol., 52, 6309–6316, https://doi.org/10.1021/acs.est.8b00538, 2018.

Bhattarai, H. R., Wanek, W., Siljanen, H. M. P., Ronkainen, J. G., Liimatainen, M., Hu, Y., Nykänen, H., Biasi, C., and Maljanen, M.: Denitrification is the major nitrous acid production pathway in boreal agricultural soils, Commun. Earth Environ., 2, 54, https://doi.org/10.1038/s43247-021-00125-7, 2021.

Chen, D. Y., Zhou, L., Liu, S., Lian, C. F., Wang, W. G., Liu, H. F., Li, C. Y., Liu, Y. L., Luo, L., Xiao, K., Chen, Y., Qiu, Y., Tan, Q. W., Ge, M. F., and Yang, F. M.: Primary sources of HONO

vary during the daytime: Insights based on a field campaign, Sci. Total Environ., 903, 12, https://doi.org/10.1016/j.scitotenv.2023.166605, 2023.

Chen, Y., Wang, W., Lian, C., Peng, C., Zhang, W., Li, J., Liu, M., Shi, B., Wang, X., and Ge, M.: Evaluation and impact factors of indoor and outdoor gas-phase nitrous acid under different environmental conditions, J. Environ. Sci. (China), 95, 165–171, https://doi.org/10.1016/j.jes.2020.03.048, 2020.

Cox, R. A., Dervent, G. K., and Holt, P. M.: Relative rate constants for the reactions of OH radicals with H_2, CH_4, CO, NO, and HONO at atmospheric pressure and 296 K, J. Chem. Soc. Faraday T., 1, 2031–2043, https://doi.org/10.1039/f19767202031, 1976.

Czader, B. H., Rappenglück, B., Percell, P., Byun, D. W., Ngan, F., and Kim, S.: Modeling nitrous acid and its impact on ozone and hydroxyl radical during the Texas Air Quality Study 2006, Atmos. Chem. Phys., 12, 6939–6951, https://doi.org/10.5194/acp-12-6939-2012, 2012.

Du, C. L., Liu, S. Y., Yu, X., Li, X. M., Chen, C., Peng, Y., Dong, Y., Dong, Z. P., and Wang, F. Q.: Urban boundary layer height characteristics and relationship with particulate matter mass concentrations in Xi'an, Central China, Aerosol Air Qual. Res., 13, 1598–1607, https://doi.org/10.4209/aaqr.2012.10.0274, 2013.

El Zein, A., Romanias, M. N., and Bedjanian, Y.: Kinetics and products of heterogeneous reaction of HONO with Fe_2O_3 and Arizona Test Dust, Environ. Sci. Technol., 47, 6325–6331, https://doi.org/10.1021/es400794c, 2013.

Elshorbany, Y. F., Kurtenbach, R., Wiesen, P., Lissi, E., Rubio, M., Villena, G., Gramsch, E., Rickard, A. R., Pilling, M. J., and Kleffmann, J.: Oxidation capacity of the city air of Santiago, Chile, Atmos. Chem. Phys., 9, 2257–2273, https://doi.org/10.5194/acp-9-2257-2009, 2009.

Elshorbany, Y. F., Steil, B., Brühl, C., and Lelieveld, J.: Impact of HONO on global atmospheric chemistry calculated with an empirical parameterization in the EMAC model, Atmos. Chem. Phys., 12, 9977–10000, https://doi.org/10.5194/acp-12-9977-2012, 2012.

Finlayson-Pitts, B. J., Wingen, L. M., Sumner, A. L., Syomin, D., and Ramazan, K. A.: The heterogeneous hydrolysis of NO_2 in laboratory systems and in outdoor and indoor atmospheres: An integrated mechanism, Phys. Chem. Chem. Phys., 5, 223–242, https://doi.org/10.1039/b208564j, 2003.

Gu, R., Shen, H., Xue, L., Wang, T., Gao, J., Li, H., Liang, Y., Xia, M., Yu, C., Liu, Y., and Wang, W.: Investigating the sources of atmospheric nitrous acid (HONO) in the megacity of Beijing, China, Sci. Total Environ., 812, 152270, https://doi.org/10.1016/j.scitotenv.2021.152270, 2022.

Hou, S., Tong, S., Ge, M., and An, J.: Comparison of atmospheric nitrous acid during severe haze and clean periods in Beijing, China, Atmos. Environ., 124, 199–206, https://doi.org/10.1016/j.atmosenv.2015.06.023, 2016.

Hu, B., Duan, J., Hong, Y., Xu, L., Li, M., Bian, Y., Qin, M., Fang, W., Xie, P., and Chen, J.: Exploration of the atmospheric chemistry of nitrous acid in a coastal city of southeastern China: results from measurements across four seasons, Atmos. Chem. Phys., 22, 371–393, https://doi.org/10.5194/acp-22-371-2022, 2022.

Huang, J., Pan, X., Guo, X., and Li, G.: Health impact of China's Air Pollution Prevention and Control Action Plan: An analysis of national air quality monitoring and mortality data, Lancet Planet. Health, 2, e313–e323, https://doi.org/10.1016/S2542-5196(18)30141-4, 2018.

Huang, R.-J., Yang, L., Cao, J., Wang, Q., Tie, X., Ho, K.-F., Shen, Z., Zhang, R., Li, G., Zhu, C., Zhang, N., Dai, W., Zhou, J., Liu, S., Chen, Y., Chen, J., and O'Dowd, C. D.: Concentration and sources of atmospheric nitrous acid (HONO) at an urban site in Western China, Sci. Total Environ., 593, 165–172, https://doi.org/10.1016/j.scitotenv.2017.02.166, 2017.

Jia, C., Tong, S., Zhang, X., Li, F., Zhang, W., Li, W., Wang, Z., Zhang, G., Tang, G., Liu, Z., and Ge, M.: Atmospheric oxidizing capacity in autumn Beijing: Analysis of the O_3 and $PM_{2.5}$ episodes based on observation-based model, J. Environ. Sci. (China), 124, 557–569, https://doi.org/10.1016/j.jes.2021.11.020, 2023.

Jia, C. H., Tong, S. R., Zhang, W. Q., Zhang, X. R., Li, W. R., Wang, Z., Wang, L. L., Liu, Z. R., Hu, B., Zhao, P. S., and Ge, M. F.: Pollution characteristics and potential sources of nitrous acid (HONO) in early autumn 2018 of Beijing, Sci. Total Environ., 735, 11, https://doi.org/10.1016/j.scitotenv.2020.139317, 2020.

Jin, S., Kong, L., Yang, K., Wang, C., Xia, L., Wang, Y., Tan, J., and Wang, L.: Combined effects of high relative humidity and ultraviolet irradiation: Enhancing the production of gaseous NO_2 from the photolysis of NH_4NO_3, Sci. Total Environ., 838, 156480, https://doi.org/10.1016/j.scitotenv.2022.156480, 2022.

Keller-Rudek, H., Moortgat, G. K., Sander, R., and Sörensen, R.: The MPI-Mainz UV/VIS Spectral Atlas of Gaseous Molecules of Atmospheric Interest, Earth Syst. Sci. Data, 5, 365–373, https://doi.org/10.5194/essd-5-365-2013, 2013.

Kessler, C. and Platt, U.: Nitrous acid in polluted air masses-Sources and formation pathways, in: Physico–Chemical Behaviour of Atmospheric Pollutants, edited by: Versino, B. and Angeletti, G., Springer, Dordrecht, https://doi.org/10.1007/978-94-009-6505-8_44, 412–422, 1984.

Kirchstetter, T. W., Harley, R. A., and Littlejohn, D.: Measurement of nitrous acid in motor vehicle exhaust, Environ. Sci. Technol., 30, 2843–2849, https://doi.org/10.1021/es960135y, 1996.

Kleffmann, J., Becker, K. H., and Wiesen, P.: Heterogeneous NO_2 conversion processes on acid surfaces: Possible atmospheric implications, Atmos. Environ., 32, 2721–2729, https://doi.org/10.1016/s1352-2310(98)00065-x, 1998.

Kurtenbach, R., Becker, K. H., Gomes, J. A. G., Kleffmann, J., Lörzer, J. C., Spittler, M., Wiesen, P., Ackermann, R., Geyer, A., and Platt, U.: Investigations of emissions and heterogeneous formation of HONO in a road traffic tunnel, Atmos. Environ., 35, 3385–3394, https://doi.org/10.1016/S1352-2310(01)00138-8, 2001.

Li, C., Hammer, M. S., Zheng, B., and Cohen, R. C.: Accelerated reduction of air pollutants in China, 2017–2020, Sci. Total Environ., 803, 150011, https://doi.org/10.1016/j.scitotenv.2021.150011, 2022.

Li, D., Xue, L., Wen, L., Wang, X., Chen, T., Mellouki, A., Chen, J., and Wang, W.: Characteristics and sources of nitrous acid in an urban atmosphere of northern China: Results from 1-yr continuous observations, Atmos. Environ., 182, 296–306, https://doi.org/10.1016/j.atmosenv.2018.03.033, 2018.

Li, X., Brauers, T., Häseler, R., Bohn, B., Fuchs, H., Hofzumahaus, A., Holland, F., Lou, S., Lu, K. D., Rohrer, F., Hu, M., Zeng, L. M., Zhang, Y. H., Garland, R. M., Su, H., Nowak, A., Wiedensohler, A., Takegawa, N., Shao, M., and Wahner, A.: Explor-

ing the atmospheric chemistry of nitrous acid (HONO) at a rural site in Southern China, Atmos. Chem. Phys., 12, 1497–1513, https://doi.org/10.5194/acp-12-1497-2012, 2012.

Li, Y., Wang, X., Wu, Z., Li, L., Wang, C., Li, H., Zhang, X., Zhang, Y., Li, J., Gao, R., Xue, L., Mellouki, A., Ren, Y., and Zhang, Q.: Atmospheric nitrous acid (HONO) in an alternate process of haze pollution and ozone pollution in urban Beijing in summertime: Variations, sources and contribution to atmospheric photochemistry, Atmos. Res., 260, 105689, https://doi.org/10.1016/j.atmosres.2021.105689, 2021.

Lian, C., Wang, W., Chen, Y., Zhang, Y., Zhang, J., Liu, Y., Fan, X., Li, C., Zhan, J., Lin, Z., Hua, C., Zhang, W., Liu, M., Li, J., Wang, X., An, J., and Ge, M.: Long-term winter observation of nitrous acid in the urban area of Beijing, J. Environ. Sci. (China), 114, 334–342, https://doi.org/10.1016/j.jes.2021.09.010, 2022.

Liao, S., Zhang, J., Yu, F., Zhu, M., Liu, J., Ou, J., Dong, H., Sha, Q., Zhong, Z., Xie, Y., Luo, H., Zhang, L., and Zheng, J.: High gaseous nitrous acid (HONO) emissions from light-duty diesel vehicles, Environ. Sci. Technol., 55, 200–208, https://doi.org/10.1021/acs.est.0c05599, 2021.

Lin, D., Tong, S., Zhang, W., Li, W., Li, F., Jia, C., Zhang, G., Chen, M., Zhang, X., Wang, Z., Ge, M., and He, X.: Formation mechanisms of nitrous acid (HONO) during the haze and non-haze periods in Beijing, China, J. Environ. Sci. (China), 114, 343–353, https://doi.org/10.1016/j.jes.2021.09.013, 2022.

Liu, J., Liu, Z., Ma, Z., Yang, S., Yao, D., Zhao, S., Hu, B., Tang, G., Sun, J., Cheng, M., Xu, Z., and Wang, Y.: Detailed budget analysis of HONO in Beijing, China: Implication on atmosphere oxidation capacity in polluted megacity, Atmos. Environ., 244, 117957, https://doi.org/10.1016/j.atmosenv.2020.117957, 2021.

Liu, J. P., Deng, H. F., Li, S., Jiang, H. Y., Mekic, M., Zhou, W. T., Wang, Y. Q., Loisel, G., Wang, X. M., and Gligorovski, S.: Light-enhanced heterogeneous conversion of NO_2 to HONO on solid films consisting of Fluorene and Fluorene/Na_2SO_4: An impact on urban and indoor atmosphere, Environ. Sci. Technol., 54, 11079–11086, https://doi.org/10.1021/acs.est.0c02627, 2020.

Liu, J. P., Li, B., Deng, H. F., Yang, Y., Song, W., Wang, X. M., Luo, Y. M., Francisco, J. S., Li, L., and Gligorovski, S.: Resolving the formation mechanism of HONO via Ammonia-Promoted photosensitized conversion of monomeric NO_2 on urban glass surfaces, J. Am. Chem. Soc., 145, 11488–11493, https://doi.org/10.1021/jacs.3c02067, 2023.

Liu, Y., Nie, W., Xu, Z., Wang, T., Wang, R., Li, Y., Wang, L., Chi, X., and Ding, A.: Semi-quantitative understanding of source contribution to nitrous acid (HONO) based on 1 year of continuous observation at the SORPES station in eastern China, Atmos. Chem. Phys., 19, 13289–13308, https://doi.org/10.5194/acp-19-13289-2019, 2019.

Liu, Y., Geng, G., Cheng, J., Liu, Y., Xiao, Q., Liu, L., Shi, Q., Tong, D., He, K., and Zhang, Q.: Drivers of increasing ozone during the two phases of Clean Air Actions in China 2013-2020, Environ. Sci. Technol., 57, 8954–8964, https://doi.org/10.1021/acs.est.3c00054, 2023.

Liu, Z., Wang, Y., Hu, B., Lu, K., Tang, G., Ji, D., Yang, X., Gao, W., Xie, Y., Liu, J., Yao, D., Yang, Y., and Zhang, Y.: Elucidating the quantitative characterization of atmospheric oxidation capacity in Beijing, China, Sci. Total Environ., 771, 145306, https://doi.org/10.1016/j.scitotenv.2021.145306, 2021.

Murthy, B. S., Latha, R., Tiwari, A., Rathod, A., Singh, S., and Beig, G.: Impact of mixing layer height on air quality in winter, J. Atmos. Sol.-Terr. Phy., 197, 105157, https://doi.org/10.1016/j.jastp.2019.105157, 2020.

Nie, W., Ding, A. J., Xie, Y. N., Xu, Z., Mao, H., Kerminen, V.-M., Zheng, L. F., Qi, X. M., Huang, X., Yang, X.-Q., Sun, J. N., Herrmann, E., Petäjä, T., Kulmala, M., and Fu, C. B.: Influence of biomass burning plumes on HONO chemistry in eastern China, Atmos. Chem. Phys., 15, 1147–1159, https://doi.org/10.5194/acp-15-1147-2015, 2015.

Pinto, J. P., Dibb, J., Lee, B. H., Rappenglück, B., Wood, E. C., Levy, M., Zhang, R. Y., Lefer, B., Ren, X. R., Stutz, J., Tsai, C., Ackermann, L., Golovko, J., Herndon, S. C., Oakes, M., Meng, Q. Y., Munger, J. W., Zahniser, M., and Zheng, J.: Intercomparison of Field Measurements of Nitrous Acid (HONO) during the SHARP Campaign, J. Geophys. Res.-Atmos., 119, 5583–5601, https://doi.org/10.1002/2013JD020287, 2014.

Ren, Y., Wei, J., Wang, G., Wu, Z., Ji, Y., and Li, H.: Evolution of aerosol chemistry in Beijing under strong influence of anthropogenic pollutants: Composition, sources, and secondary formation of fine particulate nitrated aromatic compounds, Environ. Res., 204, 111982, https://doi.org/10.1016/j.envres.2021.111982, 2022.

Requia, W. J., Higgins, C. D., Adams, M. D., Mohamed, M., and Koutrakis, P.: The health impacts of weekday traffic: A health risk assessment of $PM_{2.5}$ emissions during congested periods, Environ. Int., 111, 164–176, https://doi.org/10.1016/j.envint.2017.11.025, 2018.

Romanias, M. N., El Zein, A., and Bedjanian, Y.: Reactive uptake of HONO on aluminium oxide surface, J. Photoch. Photobio. A, 250, 50–57, https://doi.org/10.1016/j.jphotochem.2012.09.018, 2012.

Rohrer, F. and Berresheim, H.: Strong correlation between levels of tropospheric hydroxyl radicals and solar ultraviolet radiation, Nature, 442, 184–187, https://doi.org/10.1038/nature04924, 2006.

Rohrer, F., Lu, K., Hofzumahaus, A., Bohn, B., Brauers, T., Chang, C.-C., Fuchs, H., Häseler, R., Holland, F., Hu, M., Kita, K., Kondo, Y., Li, X., Lou, S., Oebel, A., Shao, M., Zeng, L., Zhu, T., Zhang, Y., and Wahner, A.: Maximum efficiency in the hydroxyl radical-based self-cleansing of the troposphere, Nat. Geosci., 7, 559–563, https://doi.org/10.1038/ngeo2199, 2014.

Simoneit, B. R. T.: Biomass burning – A review of organic tracers for smoke from incomplete combustion, Appl. Geochem., 17, 129–162, https://doi.org/10.1016/S0883-2927(01)00061-0, 2002.

Sörgel, M., Regelin, E., Bozem, H., Diesch, J.-M., Drewnick, F., Fischer, H., Harder, H., Held, A., Hosaynali-Beygi, Z., Martinez, M., and Zetzsch, C.: Quantification of the unknown HONO daytime source and its relation to NO_2, Atmos. Chem. Phys., 11, 10433–10447, https://doi.org/10.5194/acp-11-10433-2011, 2011.

Song, M., Zhao, X., Liu, P., Mu, J., He, G., Zhang, C., Tong, S., Xue, C., Zhao, X., Ge, M., and Mu, Y.: Atmospheric NO_x oxidation as major sources for nitrous acid (HONO), npj Clim. Atmos. Sci., 6, 30, https://doi.org/10.1038/s41612-023-00357-8, 2023.

Spataro, F., Ianniello, A., Esposito, G., Allegrini, I., Zhu, T., and Hu, M.: Occurrence of atmospheric nitrous acid in the urban

area of Beijing (China), Sci. Total Environ., 447, 210–224, https://doi.org/10.1016/j.scitotenv.2012.12.065, 2013.

Stolzenburg, D., Cai, R., Blichner, S. M., Kontkanen, J., Zhou, P., Makkonen, R., Kerminen, V.-M., Kulmala, M., Riipinen, I., and Kangasluoma, J.: Atmospheric nanoparticle growth, Rev. Mod. Phys., 95, 045002, https://doi.org/10.1103/RevModPhys.95.045002, 2023.

Stutz, J., Alicke, B., and Neftel, A.: Nitrous acid formation in the urban atmosphere: Gradient measurements of NO_2 and HONO over grass in Milan, Italy, J. Geophys. Res.-Atmos., 107, 8192, https://doi.org/10.1029/2001JD000390, 2002.

Su, H., Cheng, Y. F., Shao, M., Gao, D. F., Yu, Z. Y., Zeng, L. M., Slanina, J., Zhang, Y. H., and Wiedensohler, A.: Nitrous acid (HONO) and its daytime sources at a rural site during the 2004 PRIDE-PRD experiment in China, J. Geophys. Res.-Atmos., 113, D14312, https://doi.org/10.1029/2007jd009060, 2008.

Su, H., Cheng, Y., Oswald, R., Behrendt, T., Trebs, I., Meixner, F. X., Andreae, M. O., Cheng, P., Zhang, Y., and Pöschl, U.: Soil nitrite as a source of atmospheric HONO and OH radical, Science, 333, 1616–1618, https://doi.org/10.1126/science.1207687, 2011.

Tan, Z., Fuchs, H., Lu, K., Hofzumahaus, A., Bohn, B., Broch, S., Dong, H., Gomm, S., Häseler, R., He, L., Holland, F., Li, X., Liu, Y., Lu, S., Rohrer, F., Shao, M., Wang, B., Wang, M., Wu, Y., Zeng, L., Zhang, Y., Wahner, A., and Zhang, Y.: Radical chemistry at a rural site (Wangdu) in the North China Plain: observation and model calculations of OH, HO_2 and RO_2 radicals, Atmos. Chem. Phys., 17, 663–690, https://doi.org/10.5194/acp-17-663-2017, 2017.

Tan, Z., Rohrer, F., Lu, K., Ma, X., Bohn, B., Broch, S., Dong, H., Fuchs, H., Gkatzelis, G. I., Hofzumahaus, A., Holland, F., Li, X., Liu, Y., Liu, Y., Novelli, A., Shao, M., Wang, H., Wu, Y., Zeng, L., Hu, M., Kiendler-Scharr, A., Wahner, A., and Zhang, Y.: Wintertime photochemistry in Beijing: observations of RO_x radical concentrations in the North China Plain during the BEST-ONE campaign, Atmos. Chem. Phys., 18, 12391–12411, https://doi.org/10.5194/acp-18-12391-2018, 2018.

Tong, S., Hou, S., Zhang, Y., Chu, B., Liu, Y., He, H., Zhao, P., and Ge, M.: Comparisons of measured nitrous acid (HONO) concentrations in a pollution period at urban and suburban Beijing, in autumn of 2014, Sci. China Chem., 58, 1393–1402, https://doi.org/10.1007/s11426-015-5454-2, 2015.

VandenBoer, T. C., Brown, S. S., Murphy, J. G., Keene, W. C., Young, C. J., Pszenny, A. A. P., Kim, S., Warneke, C., de Gouw, J., Maben, J. R., Wagner, N. L., Riedel, T. P., Thornton, J. A., Wolfe, D. E., Dubé, W. P., Öztürk, F., Brock, C. A., Grossberg, N., Lefer, B., Lerner, B. M., Middlebrook, A. M., and Roberts, J. M.: Understanding the role of the ground surface in HONO vertical structure: High resolution vertial profiles during NACHTT-11, J. Geophys. Res., 118, 10155–10171, 2013.

VandenBoer, T. C., Young, C. J., Talukdar, R. K., Markovic, M. Z., Brown, S. S., Roberts, J. M., and Murphy, J. G.: Nocturnal loss and daytime source of nitrous acid through reactive uptake and displacement, Nat. Geosci., 8, 55–60, https://doi.org/10.1038/ngeo2298, 2015.

Veres, P. R., Roberts, J. M., Wild, R. J., Edwards, P. M., Brown, S. S., Bates, T. S., Quinn, P. K., Johnson, J. E., Zamora, R. J., and de Gouw, J.: Peroxynitric acid (HO_2NO_2) measurements during the UBWOS 2013 and 2014 studies using iodide ion chemical ionization mass spectrometry, Atmos. Chem. Phys., 15, 8101–8114, https://doi.org/10.5194/acp-15-8101-2015, 2015.

Wang, J., Zhang, X., Guo, J., Wang, Z., and Zhang, M.: Observation of nitrous acid (HONO) in Beijing, China: Seasonal variation, nocturnal formation and daytime budget, Sci. Total Environ., 587–588, 350–359, https://doi.org/10.1016/j.scitotenv.2017.02.159, 2017.

Wang, J., Gao, J., Che, F., Yang, X., Yang, Y., Liu, L., Xiang, Y., and Li, H.: Summertime response of ozone and fine particulate matter to mixing layer meteorology over the North China Plain, Atmos. Chem. Phys., 23, 14715–14733, https://doi.org/10.5194/acp-23-14715-2023, 2023.

Wang, J. Q., Gao, J., Che, F., Wang, Y. L., Lin, P. C., and Zhang, Y. C.: Dramatic changes in aerosol composition during the 2016-2020 heating seasons in Beijing–Tianjin–Hebei region and its surrounding areas: The role of primary pollutants and secondary aerosol formation, Sci. Total Environ., 849, 157621, https://doi.org/10.1016/j.scitotenv.2022.157621, 2022.

Wang, S., Ackermann, R., and Stutz, J.: Vertical profiles of O_3 and NO_x chemistry in the polluted nocturnal boundary layer in Phoenix, AZ: I. Field observations by long-path DOAS, Atmos. Chem. Phys., 6, 2671–2693, https://doi.org/10.5194/acp-6-2671-2006, 2006.

Wang, T., Xue, L., Brimblecombe, P., Lam, Y. F., Li, L., and Zhang, L.: Ozone pollution in China: A review of concentrations, meteorological influences, chemical precursors, and effects, Sci. Total Environ., 575, 1582–1596, https://doi.org/10.1016/j.scitotenv.2016.10.081, 2017.

Wang, Y., Wang, J., Wang, Y., Zhang, Y., Woodward-Massey, R., Zhang, C., Kuang, Y., Zhu, J., Shang, J., Li, X., Zeng, L., Lin, W., and Ye, C.: Experimental and kinetic model evaluation of HONO production from surface nitrate photolysis, Atmos. Environ., 296, 119568, https://doi.org/10.1016/j.atmosenv.2022.119568, 2023.

Weber, B., Wu, D., Tamm, A., Ruckteschler, N., Rodríguez-Caballero, E., Steinkamp, J., Meusel, H., Elbert, W., Behrendt, T., Sörgel, M., Cheng, Y., Crutzen, P. J., Su, H., and Pöschl, U.: Biological soil crusts accelerate the nitrogen cycle through large NO and HONO emissions in drylands, P. Natl. Acad. Sci. USA, 112, 15384–15389, https://doi.org/10.1073/pnas.1515818112, 2015.

Wingen, L. M., Moskun, A. C., Johnson, S. N., Thomas, J. L., Roeselova, M., Tobias, D. J., Kleinman, M. T., and Finlayson-Pitts, B. J.: Enhanced surface photochemistry in chloride-nitrate ion mixtures, Physical chemistry chemical physics: Phys. Chem. Chem. Phys., 10, 5668–5677, https://doi.org/10.1039/b806613b, 2008.

Wong, K. W., Oh, H.-J., Lefer, B. L., Rappenglück, B., and Stutz, J.: Vertical profiles of nitrous acid in the nocturnal urban atmosphere of Houston, TX, Atmos. Chem. Phys., 11, 3595–3609, https://doi.org/10.5194/acp-11-3595-2011, 2011.

Wong, K. W., Tsai, C., Lefer, B., Haman, C., Grossberg, N., Brune, W. H., Ren, X., Luke, W., and Stutz, J.: Daytime HONO vertical gradients during SHARP 2009 in Houston, TX, Atmos. Chem. Phys., 12, 635–652, https://doi.org/10.5194/acp-12-635-2012, 2012.

Wong, K. W., Tsai, C., Lefer, B., Grossberg, N., and Stutz, J.: Modeling of daytime HONO vertical gradients during SHARP 2009, Atmos. Chem. Phys., 13, 3587–3601, https://doi.org/10.5194/acp-13-3587-2013, 2013.

Wu, D., Horn, M. A., Behrendt, T., Muller, S., Li, J., Cole, J. A., Xie, B., Ju, X., Li, G., Ermel, M., Oswald, R., Frohlich-Nowoisky, J., Hoor, P., Hu, C., Liu, M., Andreae, M. O., Poschl, U., Cheng, Y., Su, H., Trebs, I., Weber, B., and Sorgel, M.: Soil HONO emissions at high moisture content are driven by microbial nitrate reduction to nitrite: Tackling the HONO puzzle, ISME J., 13, 1688–1699, https://doi.org/10.1038/s41396-019-0379-y, 2019.

Xinghua, L., Shuxiao, W., Lei, D., Jiming, H., Chao, L., Yaosheng, C., and Yang, L.: Particulate and trace gas emissions from open burning of wheat straw and corn stover in China, Environ. Sci. Technol., 41, 6052–6058, https://doi.org/10.1021/es0705137, 2007.

Xu, W., Kuang, Y., Zhao, C., Tao, J., Zhao, G., Bian, Y., Yang, W., Yu, Y., Shen, C., Liang, L., Zhang, G., Lin, W., and Xu, X.: NH_3-promoted hydrolysis of NO_2 induces explosive growth in HONO, Atmos. Chem. Phys., 19, 10557–10570, https://doi.org/10.5194/acp-19-10557-2019, 2019.

Xu, Z., Wang, T., Wu, J. Q., Xue, L. K., Chan, J., Zha, Q. Z., Zhou, S. Z., Louie, P. K. K., and Luk, C. W. Y.: Nitrous acid (HONO) in a polluted subtropical atmosphere: Seasonal variability, direct vehicle emissions and heterogeneous production at ground surface, Atmos. Environ., 106, 100–109, https://doi.org/10.1016/j.atmosenv.2015.01.061, 2015.

Xuan, H., Zhao, Y., Ma, Q., Chen, T., Liu, J., Wang, Y., Liu, C., Wang, Y., Liu, Y., Mu, Y., and He, H.: Formation mechanisms and atmospheric implications of summertime nitrous acid (HONO) during clean, ozone pollution and double high-level $PM_{2.5}$ and O_3 pollution periods in Beijing, Sci. Total Environ., 857, 159538, https://doi.org/10.1016/j.scitotenv.2022.159538, 2023.

Xue, C., Zhang, C., Ye, C., Liu, P., Catoire, V., Krysztofiak, G., Chen, H., Ren, Y., Zhao, X., Wang, J., Zhang, F., Zhang, C., Zhang, J., An, J., Wang, T., Chen, J., Kleffmann, J., Mellouki, A., and Mu, Y.: HONO Budget and Its Role in Nitrate Formation in the Rural North China Plain, Environ. Sci. Technol., 54, 11048–11057, https://doi.org/10.1021/acs.est.0c01832, 2020.

Xue, C., Ye, C., Zhang, C., Catoire, V., Liu, P., Gu, R., Zhang, J., Ma, Z., Zhao, X., Zhang, W., Ren, Y., Krysztofiak, G., Tong, S., Xue, L., An, J., Ge, M., Mellouki, A., and Mu, Y.: Evidence for strong HONO emission from fertilized agricultural fields and its remarkable impact on regional O_3 pollution in the summer North China Plain, ACS Earth Space Chem., 5, 340–347, https://doi.org/10.1021/acsearthspacechem.0c00314, 2021.

Yang, W., Han, C., Yang, H., and Xue, X.: Significant HONO formation by the photolysis of nitrates in the presence of humic acids, Environ. Pollut., 243, 679–686, https://doi.org/10.1016/j.envpol.2018.09.039, 2018.

Yang, W., Han, C., Zhang, T., Tang, N., Yang, H., and Xue, X.: Heterogeneous photochemical uptake of NO_2 on the soil surface as an important ground-level HONO source, Environ. Pollut., 271, 116289, https://doi.org/10.1016/j.envpol.2020.116289, 2021.

Yang, X., Lu, K., Ma, X., Liu, Y., Wang, H., Hu, R., Li, X., Lou, S., Chen, S., Dong, H., Wang, F., Wang, Y., Zhang, G., Li, S., Yang, S., Yang, Y., Kuang, C., Tan, Z., Chen, X., Qiu, P., Zeng, L., Xie, P., and Zhang, Y.: Observations and modeling of OH and HO_2 radicals in Chengdu, China in summer 2019, Sci. Total Environ., 772, 144829, https://doi.org/10.1016/j.scitotenv.2020.144829, 2021.

Ye, C., Zhang, N., Gao, H., and Zhou, X.: Matrix effect on surface-catalyzed photolysis of nitric acid, Sci. Rep., 9, 4351, https://doi.org/10.1038/s41598-018-37973-x, 2019.

Ye, C. X., Zhang, N., Gao, H. L., and Zhou, X. L.: Photolysis of particulate nitrate as a source of HONO and NO_x, Environ. Sci. Technol., 51, 6849–6856, https://doi.org/10.1021/acs.est.7b00387, 2017.

Young, C. J., Washenfelder, R. A., Mielke, L. H., Osthoff, H. D., Veres, P., Cochran, A. K., VandenBoer, T. C., Stark, H., Flynn, J., Grossberg, N., Haman, C. L., Lefer, B., Gilman, J. B., Kuster, W. C., Tsai, C., Pikelnaya, O., Stutz, J., Roberts, J. M., and Brown, S. S.: Vertically resolved measurements of nighttime radical reservoirs in Los Angeles and their contribution to the urban radical budget. Environ. Sci. Technol., 46, 10965–10973, 2012.

Yu, C. A., Huang, L. B., Xue, L. K., Shen, H. Q., Li, Z. Y., Zhao, M., Yang, J., Zhang, Y. N., Li, H. Y., Mu, J. S., and Wang, W. X.: Photoenhanced heterogeneous uptake of NO_2 and HONO formation on authentic winter time urban grime, ACS Earth Space Chem., 6, 1960–1968, https://doi.org/10.1021/acsearthspacechem.2c00054, 2022.

Yu, Y., Cheng, P., Li, H., Yang, W., Han, B., Song, W., Hu, W., Wang, X., Yuan, B., Shao, M., Huang, Z., Li, Z., Zheng, J., Wang, H., and Yu, X.: Budget of nitrous acid (HONO) at an urban site in the fall season of Guangzhou, China, Atmos. Chem. Phys., 22, 8951–8971, https://doi.org/10.5194/acp-22-8951-2022, 2022.

Yun, H., Wang, Z., Zha, Q., Wang, W., Xue, L., Zhang, L., Li, Q., Cui, L., Lee, S., Poon, S. C. N., and Wang, T.: Nitrous acid in a street canyon environment: Sources and contributions to local oxidation capacity, Atmos. Environ., 167, 223–234, https://doi.org/10.1016/j.atmosenv.2017.08.018, 2017.

Zhang, J., Chen, J., Xue, C., Chen, H., Zhang, Q., Liu, X., Mu, Y., Guo, Y., Wang, D., Chen, Y., Li, J., Qu, Y., and An, J.: Impacts of six potential HONO sources on HOx budgets and SOA formation during a wintertime heavy haze period in the North China Plain, Sci. Total Environ., 681, 110–123, https://doi.org/10.1016/j.scitotenv.2019.05.100, 2019.

Zhang, J., Lian, C., Wang, W., Ge, M., Guo, Y., Ran, H., Zhang, Y., Zheng, F., Fan, X., Yan, C., Daellenbach, K. R., Liu, Y., Kulmala, M., and An, J.: Amplified role of potential HONO sources in O_3 formation in North China Plain during autumn haze aggravating processes, Atmos. Chem. Phys., 22, 3275–3302, https://doi.org/10.5194/acp-22-3275-2022, 2022.

Zhang, Q., Liu, P., Wang, Y., George, C., Chen, T., Ma, S., Ren, Y., Mu, Y., Song, M., Herrmann, H., Mellouki, A., Chen, J., Yue, Y., Zhao, X., Wang, S., and Zeng, Y.: Unveiling the underestimated direct emissions of nitrous acid (HONO), P. Natl. Acad. Sci. USA, 120, e2302048120, https://doi.org/10.1073/pnas.2302048120, 2023.

Zhang, W., Tong, S., Ge, M., An, J., Shi, Z., Hou, S., Xia, K., Qu, Y., Zhang, H., Chu, B., Sun, Y., and He, H.: Variations and sources of nitrous acid (HONO) during a severe pollution episode in Beijing in winter 2016, Sci. Total Environ., 648, 253–262, https://doi.org/10.1016/j.scitotenv.2018.08.133, 2019.

Zhang, W., Tong, S., Lin, D., Li, F., Zhang, X., Wang, L., Ji, D., Tang, G., Liu, Z., Hu, B., and Ge, M.: Atmospheric chemistry of nitrous acid and its effects on hydroxyl radical and ozone at the urban area of Beijing in early spring 2021, Environ. Pollut., 316, 120710, https://doi.org/10.1016/j.envpol.2022.120710, 2023.

Zhang, X., Li, H., Wang, X., Zhang, Y., Bi, F., Wu, Z., Liu, Y., Zhang, H., Gao, R., Xue, L., Zhang, Q., Chen, Y., Chai, F., and Wang, W.: Heavy ozone pollution episodes in urban Beijing during the early summertime from 2014 to 2017: Implications for control strategy, Environ. Pollut., 285, 117162, https://doi.org/10.1016/j.envpol.2021.117162, 2021.

Zhang, X., Tong, S., Jia, C., Zhang, W., Wang, Z., Tang, G., Hu, B., Liu, Z., Wang, L., Zhao, P., Pan, Y., and Ge, M.: Elucidating HONO formation mechanism and its essential contribution to OH during haze events, npj Clim. Atmos. Sci., 6, 55, https://doi.org/10.1038/s41612-023-00371-w, 2023.

Zhang, Y., Shindell, D., Seltzer, K., Shen, L., Lamarque, J.-F., Zhang, Q., Zheng, B., Xing, J., Jiang, Z., and Zhang, L.: Impacts of emission changes in China from 2010 to 2017 on domestic and intercontinental air quality and health effect, Atmos. Chem. Phys., 21, 16051–16065, https://doi.org/10.5194/acp-21-16051-2021, 2021.

Zhong, X., Shen, H., Zhao, M., Zhang, J., Sun, Y., Liu, Y., Zhang, Y., Shan, Y., Li, H., Mu, J., Yang, Y., Nie, Y., Tang, J., Dong, C., Wang, X., Zhu, Y., Guo, M., Wang, W., and Xue, L.: Nitrous acid budgets in the coastal atmosphere: potential daytime marine sources, Atmos. Chem. Phys., 23, 14761–14778, https://doi.org/10.5194/acp-23-14761-2023, 2023.

Zhu, T., Tang, M., Gao, M., Bi, X., Cao, J., Che, H., Chen, J., Ding, A., Fu, P., Gao, J., Gao, Y., Ge, M., Ge, X., Han, Z., He, H., Huang, R.-J., Huang, X., Liao, H., Liu, C., Liu, H., Liu, J., Liu, S. C., Lu, K., Ma, Q., Nie, W., Shao, M., Song, Y., Sun, Y., Tang, X., Wang, T., Wang, T., Wang, W., Wang, X., Wang, Z., Yin, Y., Zhang, Q., Zhang, W., Zhang, Y., Zhang, Y., Zhao, Y., Zheng, M., Zhu, B., and Zhu, J.: Recent progress in atmospheric chemistry research in China: Establishing a theoretical framework for the "Air pollution complex", Adv. Atmos. Sci., 40, 1339–1361, https://doi.org/10.1007/s00376-023-2379-0, 2023.